

# Anisotropic flows of light-flavor and charmed hadrons in Pb+Pb collisions at LHC energy

Yan-ting Feng,<sup>1</sup> Rui-qin Wang,<sup>1</sup> Feng-lan Shao,<sup>1,\*</sup> and Jun Song<sup>2,†</sup>

<sup>1</sup>*School of Physics and Physical Engineering, Qufu Normal University, Shandong 273165, China*

<sup>2</sup>*School of Physics and Electronic Engineering, Jining University, Shandong 273155, China*

We apply a constituent quark equal-velocity combination (EVC) model to study the elliptic flow ( $v_2$ ) and triangular flow ( $v_3$ ) of light-flavor and single-charmed hadrons in Pb+Pb collisions at  $\sqrt{s_{NN}} = 2.76$  and 5.02 TeV.  $v_{2,3}$  of hadrons in the EVC model can be expressed as a linear superposition of the  $v_{2,3}$  of quarks at the same velocity as that of the hadrons. We find that available experimental data for  $v_2$  and  $v_3$  of  $p$ ,  $\Lambda$ ,  $\Xi$ , and  $\Omega$  as the function of transverse momentum ( $p_T$ ) can be consistently explained by the EVC formula using a  $v_2$  of up/down quarks and a  $v_2$  of strange quarks. In comparison with  $v_2$  data of  $\phi$  at  $\sqrt{s_{NN}} = 2.76$  TeV which can be naturally explained by  $v_2$  of strange quarks, explanation of data of  $\phi$  mesons at  $\sqrt{s_{NN}} = 5.02$  TeV requires an additional contribution of two-kaon coalescence, which indicates approximately 20% influence of final-state hadronic rescattering on  $v_2$  of  $\phi$  at  $\sqrt{s_{NN}} = 5.02$  TeV. Using  $v_2$  and  $v_3$  of light-flavor quarks obtained in studying light-flavor hadrons and  $v_2$  and  $v_3$  of charm quarks determined from  $D^0$  meson data, we apply the EVC model to predict the anisotropic flows of  $D_s^+$ ,  $\Lambda_c^+$ ,  $\Xi_c^0$ , and  $\Omega_c^0$  and compare them with the available experimental data. The preliminary data for  $v_2$  of  $D^0$ ,  $D_s^+$ , and  $\Lambda_c^+$  at  $\sqrt{s_{NN}} = 5.36$  TeV are found to be naturally described by the EVC model.

## I. INTRODUCTION

In ultra-relativistic heavy-ion collisions, a state of deconfined quarks and gluons is formed, known as the quark-gluon plasma (QGP) [1, 2]. In non-central collisions, the initial anisotropic collision geometry causes anisotropic expansion of the QGP in the transverse momentum plane, which in turn leads to anisotropic emission of particles in transverse momentum space [3, 4]. This anisotropic property is measured in experiments by the harmonic flow coefficients  $v_n = \langle \cos[n(\varphi - \Psi_n)] \rangle$  in the Fourier expansion of the transverse momentum distribution of hadrons [4, 5].

There have already been many measurements of the anisotropic flow of particles produced in relativistic heavy-ion collisions at the Relativistic Heavy Ion Collider (RHIC) and Large Hadron Collider (LHC). These measurements provide rich and precise data for  $v_2$ ,  $v_3$ , and higher-order flows of light-flavor and heavy-flavor hadrons. These data and the relevant theoretical studies reveal lots of important physical properties of the QGP created in ultra-relativistic heavy-ion collisions [6–10]. An interesting phenomenon related to the hadronization of the QGP is that  $v_2$  data of light-flavor hadrons (e.g.,  $\pi$ ,  $K$ ,  $p$ ,  $\Lambda$ ) exhibit a remarkable number-of-constituent-quark (NCQ) scaling [10–14]. This scaling behavior is an indication of the quark recombination mechanism at QGP hadronization. The NCQ effect is particularly pronounced in the intermediate transverse momentum region ( $2 \lesssim p_T \lesssim 6$  GeV/c), where the enhanced baryon-to-meson ratio is also observed and can be naturally explained by the quark combination models [15–21]. Recent measurements of charmed hadrons (such as  $D^0$ ,  $D_s^+$ , and  $\Lambda_c^+$ ) in Pb+Pb collisions by CMS and ALICE collaborations have found that their anisotropic flow exhibits similar behavior to that of light-flavor hadrons [22–28], suggesting that charm quarks may undergo partial thermalization and participate in the collective expansion of the QGP.

The ALICE and CMS collaborations have reported the precise measurement of the  $v_2$  and  $v_3$  of light-flavor and single-charmed hadrons in Pb+Pb Collisions at the LHC energies [13, 14, 22–25, 29, 30]. These experimental data have been studied in various theoretical models and event generators such as AMPT model [31, 32], the viscous hydrodynamic model [33, 34], the VISHNU hybrid model [35], the Boltzmann transport equation [36], the blast-wave-Tsallis-power model (BWTPM) [37], and the HYDJET++ model [38, 39]. In this paper, we apply an equal-velocity quark combination model to systematically study  $v_2$  and  $v_3$  of light-flavor and single-charmed hadrons in Pb+Pb Collisions at  $\sqrt{s_{NN}} = 2.76$  and 5.02 TeV and put particular emphasis on the self-consistency of the quark combination mechanism in explaining the experimental data of  $v_2$  and  $v_3$  of different hadrons measured by the CMS and ALICE collaborations. The equal-velocity combination of constituent quarks gives simple formulas for hadronic flow by the linear superposition of flow of quarks, which are convenient to be tested by experimental data and meanwhile are also quite visible in explaining/exhibiting the correlations among flow of different hadrons.

\* shaoff@mail.sdu.edu.cn

† songjun2011@jnxu.edu.cn

The paper is organized as follows. In Sec. II, we present the analytical formulas of the anisotropic flow hadrons in a constituent quark equal-velocity combination model and show the  $v_2$  and  $v_3$  of hadrons as the linear superposition of quark flows. In Sec. III, we apply the EVC model to study the  $v_2$  and  $v_3$  of light-flavor hadrons  $\phi$ ,  $\Lambda$ ,  $\Xi$ ,  $\Omega$ , and  $p$  in different centralities at  $\sqrt{s_{NN}} = 2.76$  and 5.02 TeV. In Sec. IV, we study the  $v_2$  and  $v_3$  of single-charmed hadrons  $D^0$ ,  $D_s^+$ ,  $\Lambda_c^+$ ,  $\Xi_c^0$ , and  $\Omega_c^0$ , and discuss the scaling property of  $v_3$  of light-flavor quarks and charm quarks. Finally, the summary is given in Sec. V.

## II. THE ANISOTROPIC FLOWS OF HADRONS IN QCM WITH EVC

In this section, we employ a constituent quark combination model (QCM) under the equal-velocity combination (EVC) approximation[16, 40–43] to describe the production of single-charmed hadrons and derive their elliptic flow ( $v_2$ ) and triangular flow ( $v_3$ ) at mid-rapidity in heavy-ion collisions. In the EVC approximation, the hadron is formed by the combination of constituent quarks and antiquarks with the same velocity as that of the hadron. In this ideal case, the momentum vectors of quarks are parallel to those of hadrons they form, and we have  $\mathbf{p}_q = x_q \mathbf{p}_h$  where  $x_q$  is momentum fraction of quark  $q$  in the hadron  $h$ . For the production of hadrons at mid-rapidity, we define the distribution function  $f(p_T, \varphi) \equiv dN/dp_T d\varphi$  where  $p_T$  is transverse momentum and  $\varphi$  is the azimuthal angle. EVC mechanism constrains  $p_{T,q} = x_q p_{T,h}$  and  $\varphi_q = \varphi_h$ . Following the spirit of EVC model, the momentum distribution function of single-charmed hadrons can be expressed as

$$f_{M_j}(p_T, \varphi) = \kappa_{M_j} f_{q_1}(x_1 p_T, \varphi) f_{\bar{q}_2}(x_2 p_T, \varphi), \quad (1)$$

$$f_{B_j}(p_T, \varphi) = \kappa_{B_j} f_{q_1}(x_1 p_T, \varphi) f_{q_2}(x_2 p_T, \varphi) f_{q_3}(x_3 p_T, \varphi). \quad (2)$$

Here, the coefficients  $\kappa_{M_j}$  and  $\kappa_{B_j}$  are independent of the transverse momentum  $p_T$ . The momentum fractions are defined as  $x_{1,2} = m_{1,2}/(m_1 + m_2)$  for mesons  $M_j(q_1 \bar{q}_2)$ , under the momentum conservation condition  $x_1 + x_2 = 1$ , and  $x_{1,2,3} = m_{1,2,3}/(m_1 + m_2 + m_3)$  for baryons  $B_j(q_1 q_2 q_3)$ , under the momentum conservation condition  $x_1 + x_2 + x_3 = 1$ . The constituent masses of quarks are adopted as  $m_u = m_d = 0.3$  GeV,  $m_s = 0.5$  GeV, and  $m_c = 1.5$  GeV, respectively.

The azimuthal dependence of particle distribution function is expressed through the Fourier series expansion

$$f(p_T, \varphi) = f(p_T) \left[ 1 + 2 \sum_{n=1}^{\infty} v_n(p_T) \cos(n\varphi) \right], \quad (3)$$

where  $f_q(p_T)$  is independent of the azimuthal angle  $\varphi$ . The anisotropic coefficient  $v_n$  is calculated by

$$v_n(p_T) = \frac{\int f(p_T, \varphi) \cos(n\varphi) d\varphi}{\int f(p_T, \varphi) d\varphi}. \quad (4)$$

Using Eqs. (1–3), we can obtain the  $v_n(p_T)$  for the meson  $M_j(q_1 \bar{q}_2)$  and baryon  $B_j(q_1 q_2 q_3)$  and the expressions up to order  $v_n^3$  are

$$\begin{aligned} v_{n,M_j} &= \frac{\int f_{M_j}(p_T, \varphi) \cos(n\varphi) d\varphi}{\int f_{M_j}(p_T, \varphi) d\varphi} \\ &= v_{n,q_1} \left[ 1 + \sum_{k=1}^{\infty} \frac{v_{k,q_1}}{v_{n,q_1}} v_{n+k,\bar{q}_2} - 2 \sum_{k=1}^{\infty} v_{k,q_1} v_{k,\bar{q}_2} \right] \\ &+ v_{n,\bar{q}_2} \left[ 1 + \sum_{k=1}^{\infty} \frac{v_{k,\bar{q}_2}}{v_{n,\bar{q}_2}} v_{n+k,q_1} - 2 \sum_{k=1}^{\infty} v_{k,q_1} v_{k,\bar{q}_2} \right] \\ &+ \sum_{k=1}^{n-1} v_{k,q_1} v_{n-k,\bar{q}_2} + \mathcal{O}(v^4), \end{aligned} \quad (5)$$

and

$$\begin{aligned}
& v_{n,B_j} \\
&= v_{n,q_1} \left\{ 1 + \sum_{k=1}^{\infty} \frac{v_{k,q_1}}{v_{n,q_1}} (v_{n+k,q_2} + v_{n+k,q_3}) - 2 \sum_{k=1}^{\infty} (v_{k,q_2} v_{k,q_1} + v_{k,q_2} v_{k,q_3} + v_{k,q_1} v_{k,q_3}) \right. \\
&\quad \left. + \sum_{k=1}^{\infty} \sum_{m=1}^{\infty} \frac{v_{k,q_1}}{v_{n,q_1}} v_{m,q_2} (v_{m+k+n,q_3} + v_{m+k-n,q_3}) \right\} \\
&+ v_{n,q_2} \left\{ 1 + \sum_{k=1}^{\infty} \frac{v_{k,q_2}}{v_{n,q_2}} (v_{n+k,q_3} + v_{n+k,q_1}) - 2 \sum_{k=1}^{\infty} (v_{k,q_2} v_{k,q_1} + v_{k,q_2} v_{k,q_3} + v_{k,q_1} v_{k,q_3}) \right. \\
&\quad \left. + \sum_{k=1}^{\infty} \sum_{m=1}^{\infty} \frac{v_{k,q_2}}{v_{n,q_2}} v_{m,q_3} (v_{m+k+n,q_1} + v_{m+k-n,q_1}) \right\} \\
&+ v_{n,q_3} \left\{ 1 + \sum_{k=1}^{\infty} \frac{v_{k,q_3}}{v_{n,q_3}} (v_{n+k,q_1} + v_{n+k,q_2}) - 2 \sum_{k=1}^{\infty} (v_{k,q_2} v_{k,q_1} + v_{k,q_2} v_{k,q_3} + v_{k,q_1} v_{k,q_3}) \right. \\
&\quad \left. + \sum_{k=1}^{\infty} \sum_{m=1}^{\infty} \frac{v_{k,q_3}}{v_{n,q_3}} v_{m,q_1} (v_{m+k+n,q_2} + v_{m+k-n,q_2}) \right\} \\
&+ \sum_{k=1}^{n-1} (v_{k,q_1} v_{n-k,q_2} + v_{k,q_2} v_{n-k,q_3} + v_{k,q_3} v_{n-k,q_1}) + \sum_{k,m=1}^{m+k \leq n-1} v_{k,q_1} v_{m,q_2} v_{n-m-k,q_3} + \mathcal{O}(v^4). \tag{6}
\end{aligned}$$

In the above formulas, we use the abbreviation  $v_{n,q_i}$  for  $v_{n,q_i}(x_i p_T)$  with  $i = 1, 2, 3$  and  $v_{n,\bar{q}_2}$  for  $v_{n,\bar{q}_2}(x_2 p_T)$ .

From Eqs. (5) and (6), we see that  $v_n$  of hadrons have a general structure of the summation of  $v_n$  of quarks and the product of lower-order quark flows. There is a modification factor before  $v_{n,q}$  which contains complex contributions of flows of quarks at various orders even for low order flows of hadrons. In order to obtain simple formulas for hadronic flow at mid-rapidity, we should consider some approximations based on the properties of hadronic flow measured in relativistic heavy-ion collisions.

First, the experimental measurements show a very small value of  $v_{1,h} \leq 10^{-3}$  at mid-rapidity in heavy-ion collisions at both RHIC and LHC energies, [44, 45], which indicates  $v_{1,q} \approx (\frac{1}{2} \sim \frac{1}{3})v_{1,h} \leq 10^{-3}$  and can be neglected in our analysis. Second, the rough estimation for  $v_{2-5,q} \approx (\frac{1}{2} \sim \frac{1}{3})v_{2-5,h}$  is approximately  $10^{-2}$  according to experimental data of  $v_{2-5,h}$  [10–14]. Higher-power terms such as  $(v_{n,q})^{4,5}$  become negligible ( $\leq 10^{-8}$ ) and can be safely omitted from the calculations. Furthermore, we adopt a scaling relation  $v_{n,q} = a_n v_{2,q}^{n/2}$  at the quark level, which has been indicated by both experimental and theoretical studies [46–52]. Using this relation, we can estimate that the ratio  $v_{n+1,q_1} v_{n+1,q_2} / v_{n,q_1} v_{n,q_2} \sim 10^{-2}$  is very small. Consequently, correction terms with harmonic indices  $k, m > 2$  in the modification factor of  $v_{n,q_i}$  can be safely neglected. The detailed derivation of these approximations is given in Ref. [42].

Based on the above considerations, the  $v_2$  and  $v_3$  of hadrons can be significantly simplified as follows

$$v_{2,M_j} \approx v_{2,q_1} [1 + (a_4 - 2) v_{2,q_1} v_{2,\bar{q}_2}] + v_{2,\bar{q}_2} [1 + (a_4 - 2) v_{2,q_1} v_{2,\bar{q}_2}], \tag{7}$$

$$\begin{aligned}
v_{2,B_j} &\approx v_{2,q_1} \{1 + (a_4 - 2) (v_{2,q_1} v_{2,q_2} + v_{2,q_1} v_{2,q_3}) - 2v_{2,q_2} v_{2,q_3}\} \\
&\quad + v_{2,q_2} \{1 + (a_4 - 2) (v_{2,q_1} v_{2,q_2} + v_{2,q_2} v_{2,q_3}) - 2v_{2,q_1} v_{2,q_3}\} \\
&\quad + v_{2,q_3} \{1 + (a_4 - 2) (v_{2,q_1} v_{2,q_3} + v_{2,q_2} v_{2,q_3}) - 2v_{2,q_2} v_{2,q_1}\}, \tag{8}
\end{aligned}$$

$$v_{3,M_j} \approx v_{3,q_1} \left[ 1 + \left( \frac{a_5}{a_3} - 2 \right) v_{2,q_1} v_{2,\bar{q}_2} \right] + v_{3,\bar{q}_2} \left[ 1 + \left( \frac{a_5}{a_3} - 2 \right) v_{2,q_1} v_{2,\bar{q}_2} \right], \tag{9}$$

$$\begin{aligned}
v_{3,B_j} &\approx v_{3,q_1} \left\{ 1 + \left( \frac{a_5}{a_3} - 2 \right) (v_{2,q_1} v_{2,q_2} + v_{2,q_1} v_{2,q_3}) - 2v_{2,q_2} v_{2,q_3} \right\} \\
&\quad + v_{3,q_2} \left\{ 1 + \left( \frac{a_5}{a_3} - 2 \right) (v_{2,q_1} v_{2,q_2} + v_{2,q_2} v_{2,q_3}) - 2v_{2,q_1} v_{2,q_3} \right\} \\
&\quad + v_{3,q_3} \left\{ 1 + \left( \frac{a_5}{a_3} - 2 \right) (v_{2,q_1} v_{2,q_3} + v_{2,q_2} v_{2,q_3}) - 2v_{2,q_2} v_{2,q_1} \right\}. \tag{10}
\end{aligned}$$

### III. THE ANISOTROPY FLOW OF LIGHT-FLAVOR HADRONS

In this section, we employ the formulas of anisotropic flow of hadrons in EVC model presented in above section to study the  $p_T$  dependence of the  $v_2$  and  $v_3$  for light-flavor hadrons  $\phi$ ,  $\Lambda$  ( $\Lambda + \bar{\Lambda}$ ),  $\Xi$  ( $\Xi^- + \bar{\Xi}^+$ ),  $\Omega$  ( $\Omega^- + \bar{\Omega}^+$ ), and  $p$  ( $p + \bar{p}$ ) at mid-rapidity in different centralities in Pb+Pb collisions at  $\sqrt{s_{NN}} = 2.76$  and 5.02 TeV.

#### A. THE ELLIPTIC FLOW OF LIGHT-FLAVOR HADRONS

In the  $v_2$  of light-flavor hadrons in Eqs. (7) and (8), there is the contribution from the quadratic term of quark  $v_2$ . In previous study [42], we estimated  $a_4 \approx 2$  using the experimental data of  $v_2$  of hadrons in Au+Au collisions at  $\sqrt{s_{NN}} = 200$  GeV [10–14]. The magnitude of  $(a_4 - 2)v_{2,q}^2$  in the modification term is therefore very small, and its contribution can be safely neglected. Consequently, the expression for the  $v_2$  of light-flavor hadrons can be simplified as follows

$$v_{2,M_j}(p_T) \approx v_{2,q_1}(x_1 p_T) + v_{2,\bar{q}_2}(x_2 p_T), \quad (11)$$

$$v_{2,B_j}(p_T) \approx v_{2,q_1}(x_1 p_T) + v_{2,q_2}(x_2 p_T) + v_{2,q_3}(x_3 p_T). \quad (12)$$

Using the simplified expressions from Eqs. (11) and (12), we obtain the following analytic formulas for the  $v_2$  of the various hadrons

$$v_{2,p}(p_T) = 3v_{2,u}(p_T/3), \quad (13)$$

$$v_{2,\Omega}(p_T) = 3v_{2,s}(p_T/3), \quad (14)$$

$$v_{2,\phi}(p_T) = 2v_{2,s}(p_T/2), \quad (15)$$

$$v_{2,\Lambda}(p_T) = 2v_{2,u}\left(\frac{1}{2 + r_{su}}p_T\right) + v_{2,s}\left(\frac{r_{su}}{2 + r_{su}}p_T\right), \quad (16)$$

$$v_{2,\Xi}(p_T) = 2v_{2,s}\left(\frac{r_{su}}{1 + 2r_{su}}p_T\right) + v_{2,u}\left(\frac{1}{1 + 2r_{su}}p_T\right). \quad (17)$$

Here, we assume the approximate isospin symmetry between up and down quarks, i.e.,  $v_{2,u} = v_{2,d}$ , and strangeness neutrality, i.e.,  $v_{2,s} = v_{2,\bar{s}}$ , in the mid-rapidity region. The relative momentum ratio  $r_{su} = m_s/m_u$  represents the constituent mass ratio between strange and up quarks. Considering uncertainties in constituent quark masses, e.g.,  $m_s = 0.5\text{--}0.55$  GeV and  $m_u = 0.3\text{--}0.33$  GeV, the derived ratio  $r_{su}$  retains an approximate value of 5/3, with an estimated uncertainty of approximately 10%. Our numerical results show that the  $v_2$  of hadrons is not sensitive to such variations in  $r_{su}$ . Consequently, this study focuses exclusively on presenting calculated  $v_2$  for hadrons using a fixed value of  $r_{su} = 1.67$ , which serves as a representative benchmark for our model predictions.

In Eqs. (13)–(17), we have only two inputs  $v_{2,u}$  and  $v_{2,s}$ , which can be fixed by fitting the experimental data for  $v_2$  of  $\Lambda$  and  $\Xi$  [13, 29] by Eq. (16) and (17), respectively. If data of  $\Xi$  are unavailable such as those in the 0–5% and 5–10% centralities at  $\sqrt{s_{NN}} = 5.02$  TeV, the values of  $v_{2,u}$  and  $v_{2,s}$  are extracted using the available data for  $\Lambda$  and  $p$  in these centralities.  $v_2$  of quarks is parameterized as

$$v_{2,q}(p_T) = a_q \exp\left[-\frac{p_T}{b_q} - c_q \exp\left(-\frac{p_T}{d_q}\right)\right], \quad (18)$$

where  $a_q$ ,  $b_q$ ,  $c_q$ , and  $d_q$  are parameters that control the shape of  $v_2$  of quarks. The extracted results for the  $v_2$  of quarks in central 0–5% to semi-central 40–50% in Pb+Pb collisions at  $\sqrt{s_{NN}} = 2.76$  and 5.02 TeV are shown in Fig. 1. The shadow areas show the statistical uncertainties, which are passed from the statistical uncertainties of the experimental data for  $\Lambda$ ,  $\Xi$  or  $\Lambda$ ,  $p$ .

In Figs. 2–3, we show the results for the  $v_2$  of the light-flavor hadrons  $\phi$ ,  $\Lambda$ ,  $\Xi$ ,  $\Omega$ , and  $p$  at mid-rapidity in different centralities (0–5%, 5–10%, 10–20%, 20–30%, 30–40%, and 40–50%) and compare them with the experimental data in Pb+Pb collisions at  $\sqrt{s_{NN}} = 2.76$  and 5.02 TeV. The QCM results are lines and experimental data [13, 29] are symbols. The experimental data of  $\Lambda$  and  $\Xi$  in the 10–20%, 20–30%, 30–40%, and 40–50% centralities at  $\sqrt{s_{NN}} = 2.76$  and 5.02 TeV are used to constrain the quark  $v_2$ , while in 0–5% and 5–10% centralities at  $\sqrt{s_{NN}} = 5.02$  TeV, the data for  $\Lambda$  and  $p$  are used. The  $v_2$  of other hadrons are theoretical predictions.

We see that the agreement between QCM results for light-flavor hadrons and experimental data is generally well. An exception is  $\phi$  mesons at  $\sqrt{s_{NN}} = 5.02$  TeV where theoretical results are below the experimental data to a certain extent. This indicates other production channels may contribute to  $\phi$  mesons production in heavy-ion collisions at  $\sqrt{s_{NN}} = 5.02$  TeV. Here, we consider the coalescence of two kaons ( $KK \rightarrow \phi$ ) at the hadronic rescattering

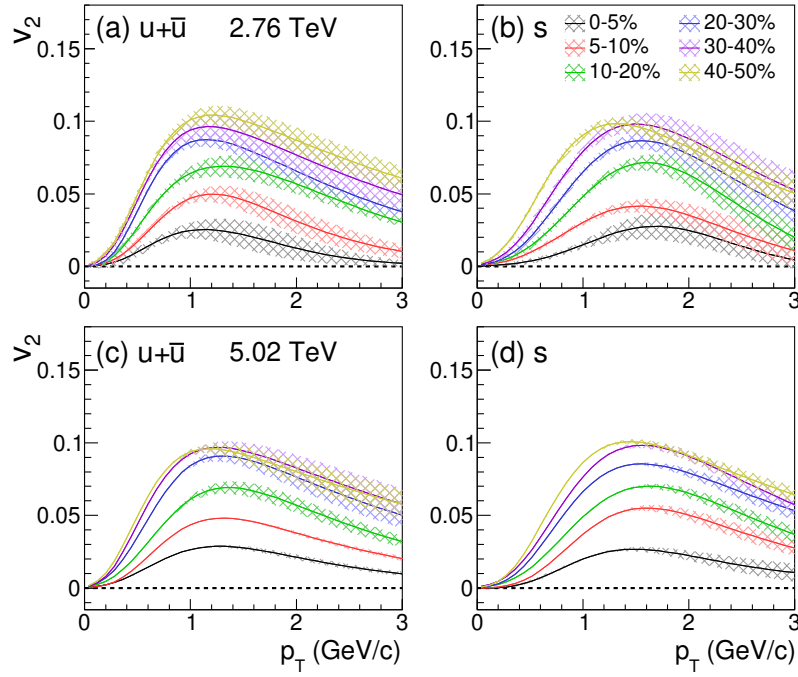


Figure 1.  $v_2$  of quarks as a function of  $p_T$  in different centralities in Pb+Pb collisions at  $\sqrt{s_{NN}}=2.76$  and 5.02 TeV.

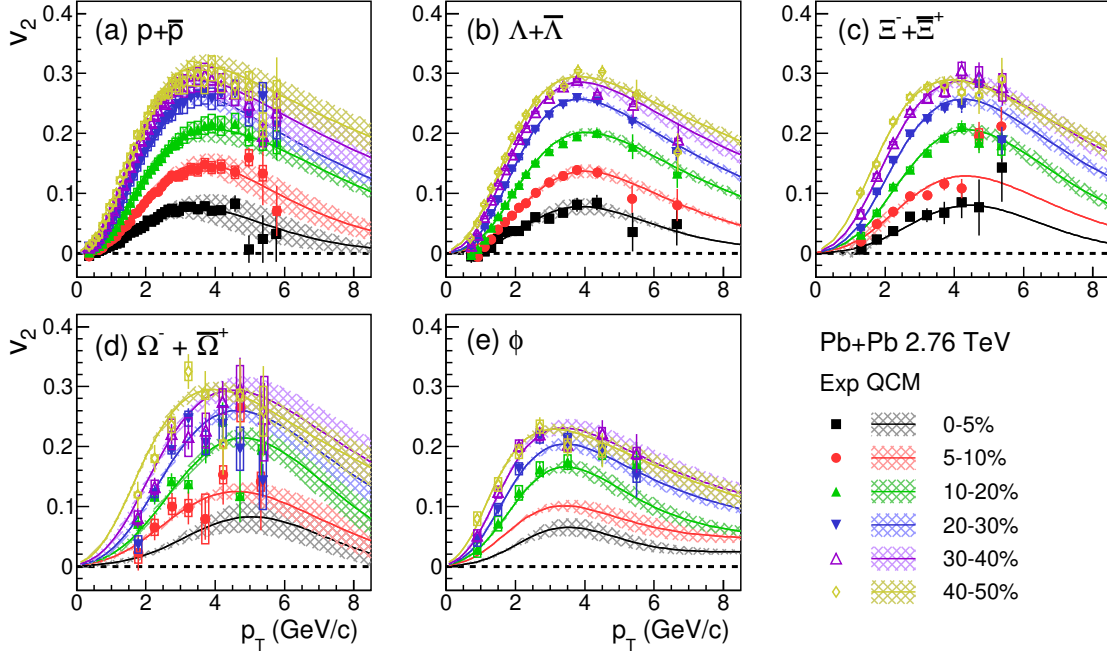


Figure 2. The  $v_2$  of (a)  $p$ , (b)  $\Lambda$ , (c)  $\Xi$ , (d)  $\Omega$ , and (e)  $\phi$  in different centralities in Pb+Pb collisions at  $\sqrt{s_{NN}}=2.76$  TeV. Symbols are the experimental data [13] and lines are model results.

stage [45, 53, 54] as a new channel of  $\phi$  meson production besides the normal quark combination at hadronization. Accordingly, the final distribution of  $\phi$  meson is modeled by incorporating both production mechanisms

$$f_{\phi}^{(final)}(p_T, \varphi) = f_{\phi, s\bar{s}}(p_T, \varphi) + f_{\phi, KK}(p_T, \varphi).$$

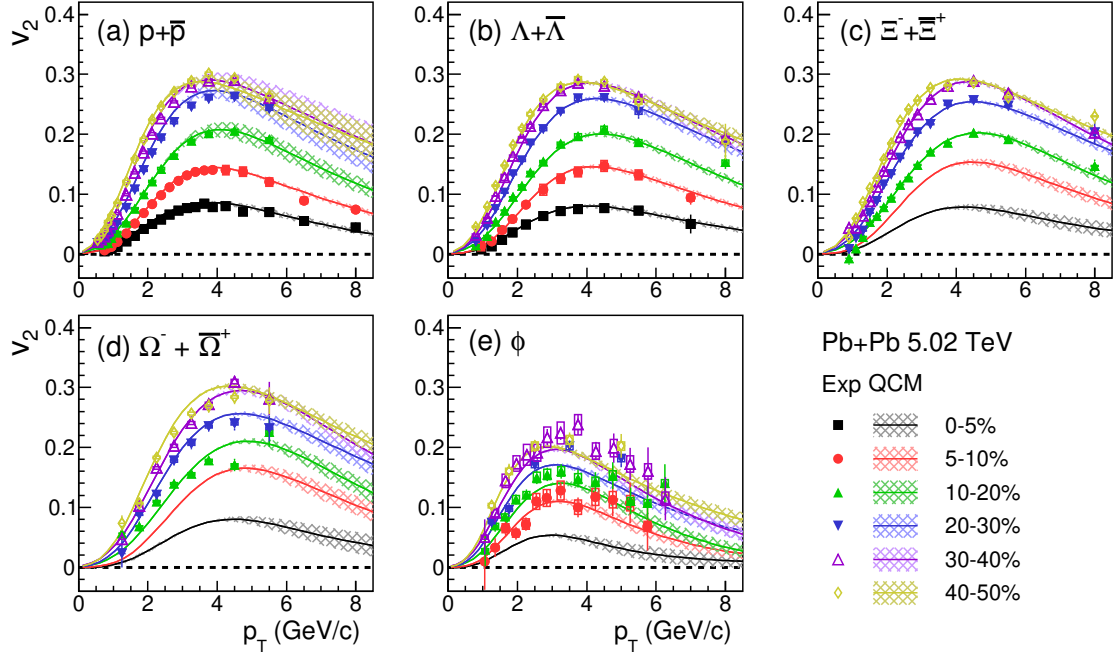


Figure 3. The  $v_2$  of (a)  $p$ , (b)  $\Lambda$ , (c)  $\Xi$ , (d)  $\Omega$ , and (e)  $\phi$  in different centralities in Pb+Pb collisions at  $\sqrt{s_{NN}} = 5.02$  TeV. Symbols are the experimental data [29, 30] and lines are model results.

The elliptic flow is

$$v_{2,\phi}^{(final)}(p_T) = (1 - z)v_{2,s\bar{s}}(p_T) + zv_{2,KK}(p_T), \quad (19)$$

where the parameter  $z$  denotes the fractional contribution of the two-kaon coalescence channel and is given by  $z = \frac{f_{\phi,KK}(p_T)}{f_{\phi,s\bar{s}}(p_T) + f_{\phi,KK}(p_T)}$ .

In Fig. 4, we apply Eq. (19) to study  $v_2$  of  $\phi$  mesons and compare theoretical calculations with experimental data [29]. The results for the pure  $s\bar{s}$  quark combination mechanism, labeled as “ $s\bar{s}$ ”, are shown as dashed curves in Fig. 4. We see that this mechanism can describe the  $v_2$  of the  $\phi$  mesons in the low transverse momentum region ( $p_T \lesssim 2.5$  GeV/c) but underestimates the data in the intermediate transverse momentum region ( $p_T \gtrsim 2.5$  GeV/c). If we introduce the channel of two-kaon coalescence ( $KK \rightarrow \phi$ ) with a contribution fraction  $z = 0.2$ , we find that the final results (the solid lines) are in good agreement with experimental data in 5-10%, 10-20%, and 20-30% centralities in Pb+Pb collisions at  $\sqrt{s_{NN}} = 5.02$  TeV. This indicates that approximately 20% of  $\phi$  meson comes from the two-kaon coalescence at hadronic rescattering state in Pb+Pb collisions at  $\sqrt{s_{NN}} = 5.02$  TeV. In semi-central collisions such as 30-40% and 40-50% centralities shown in Fig. 4 (e) and (f), 20% contribution from two-kaon coalescence is slightly overestimated and 15% is more fitted to experimental data.

## B. THE TRIANGULAR FLOW OF LIGHT-FLAVOR HADRONS

We further study the  $v_3$  of light-flavor hadrons  $\phi$ ,  $\Lambda$ ,  $\Xi$ ,  $\Omega$ , and  $p$  at mid-rapidity in different centralities in Pb+Pb collisions at  $\sqrt{s_{NN}} = 5.02$  TeV [14, 30].  $v_3$  of light-flavor hadrons in Eqs. (9) and (10) contains the contribution of the quadratic term of quark  $v_2$ . According to the NCQ estimation of the 2 – 5<sup>th</sup> flow of hadrons [10–14], the  $a_5/a_3$  is about 2.5 [46–49, 55]. Therefore, the magnitude of the  $(a_5/a_3 - 2)v_{2,q}^2$  is about  $10^{-3}$  and its influence can be neglected in the formula, and we finally obtain

$$v_{3,M_j}(p_T) \approx v_{3,q_1}(x_1 p_T) + v_{3,\bar{q}_2}(x_2 p_T), \quad (20)$$

$$v_{3,B_j}(p_T) \approx v_{3,q_1}(x_1 p_T) + v_{3,q_2}(x_2 p_T) + v_{3,q_3}(x_3 p_T). \quad (21)$$

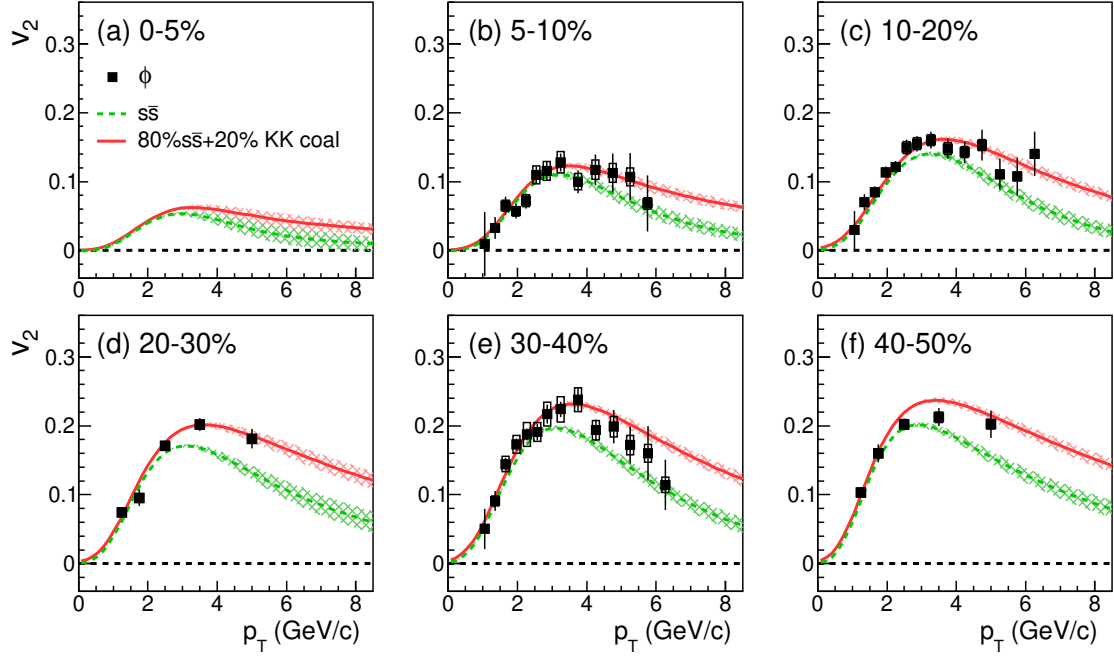


Figure 4. The  $v_2$  of  $\phi$  mesons as a function of  $p_T$  in Pb+Pb collisions at  $\sqrt{s_{NN}} = 5.02$  TeV. Experimental data (symbols) are from Refs. [29, 30]. Theoretical results including only the  $s\bar{s}$  combination are shown as dashed lines and those incorporating both  $s\bar{s}$  combination and two-kaon coalescence are shown as solid lines.

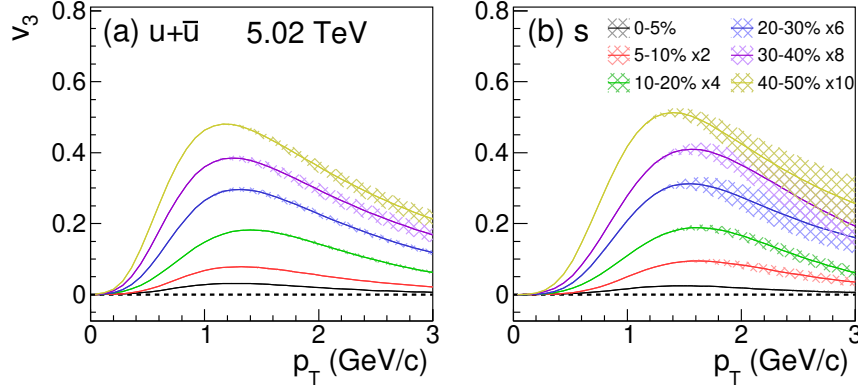


Figure 5.  $v_3$  of quarks as a function of  $p_T$  in different centralities in Pb+Pb collisions at  $\sqrt{s_{NN}} = 5.02$  TeV.

Applying Eqs. (20–21), we obtain

$$v_{3,p}(p_T) = 3v_{3,u}(p_T/3), \quad (22)$$

$$v_{3,\Omega}(p_T) = 3v_{3,s}(p_T/3), \quad (23)$$

$$v_{3,\phi}(p_T) = v_{3,s}(p_T/2) + v_{3,\bar{s}}(p_T/2), \quad (24)$$

$$v_{3,\Lambda}(p_T) = 2v_{3,u}\left(\frac{1}{2+r_{su}}p_T\right) + v_{3,s}\left(\frac{r_{su}}{2+r_{su}}p_T\right), \quad (25)$$

$$v_{3,\Xi}(p_T) = 2v_{3,s}\left(\frac{r_{su}}{1+2r_{su}}p_T\right) + v_{3,u}\left(\frac{1}{1+2r_{su}}p_T\right). \quad (26)$$

Here, we also assume the approximate isospin symmetry ( $v_{3,u} = v_{3,d}$ ) and strangeness neutrality ( $v_{3,s} = v_{3,\bar{s}}$ ) at mid-rapidity in Pb+Pb collisions at LHC energies.

We adopt an approach similar to that used for the hadronic  $v_2$  in the previous section to test EVC model. First, we adopt the formula in Eq. (18) to parameterize the  $v_3$  of (anti-)quarks, and then extract the up/down quark  $v_{3,u}$  and strange quark  $v_{3,s}$  by fitting experimental data of  $p$  and  $\Lambda$  measured in Pb+Pb collisions at LHC energies. Results

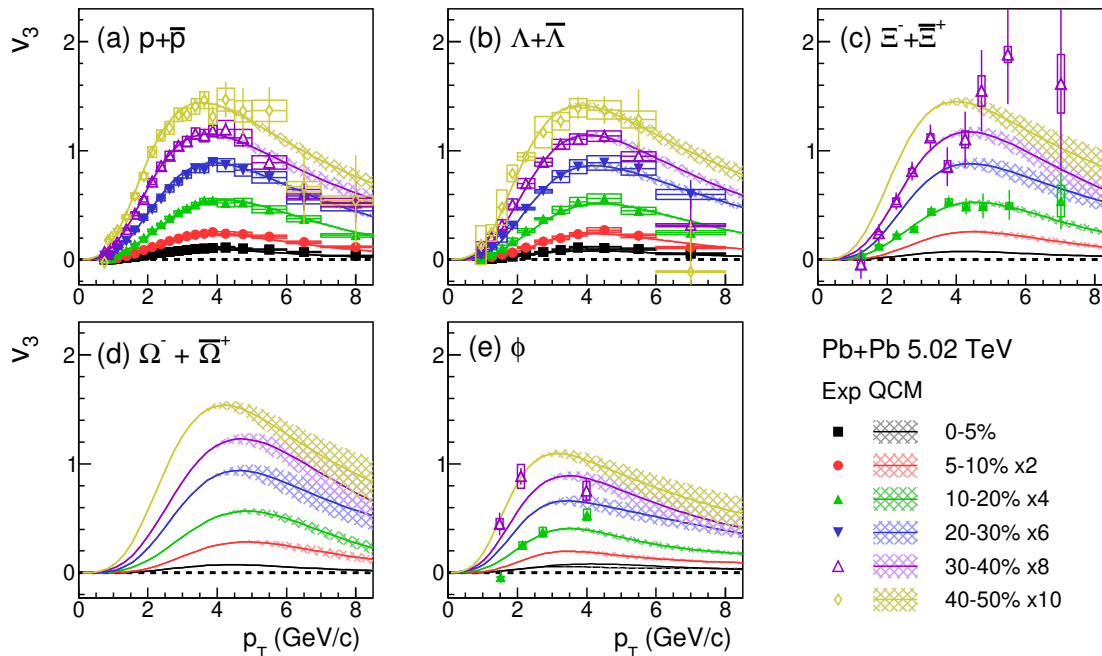


Figure 6. The  $v_3$  of (a)  $p$ , (b)  $\Lambda$ , (c)  $\Xi^- + \Xi^+$ , (d)  $\Omega^- + \Omega^+$ , and (e)  $\phi$  in different centralities in Pb+Pb collisions at  $\sqrt{s_{NN}} = 5.02$  TeV. Symbols are the experimental data [14, 30] and lines are model results.

are shown in Fig. 5, where data from different centralities are scaled by different factors for clarity. We further use the obtained  $v_{3,q}$  to calculate the  $v_3$  of other hadrons (such as  $\Xi$ ,  $\Omega$ , and  $\phi$ ) and compare them with corresponding experimental data. Fig. 6 shows the results for the  $v_3$  of  $\phi$ ,  $\Lambda$ ,  $\Xi$ ,  $\Omega$ , and  $p$  in 0-5%, 5-10%, 10-20%, 20-30%, 30-40%, 40-50% centralities in Pb+Pb collisions at  $\sqrt{s_{NN}} = 5.02$  TeV. Experimental data of the  $v_3$  of these hadrons are shown as symbols in Fig. 6 and are taken from Refs. [14, 30]. In the calculation of  $\phi$  mesons, we also consider the contribution of two-kaon coalescence to  $v_3$  of  $\phi$  and set  $z = 0.2$  in the final prediction.

Compared with the data points of  $v_2$  for hadrons, the data points of  $v_3$  for hadrons are relatively fewer. By comparing between the theoretical results and those limited experimental data, we see that theoretical calculations of  $v_3$  of  $\Xi$  and  $\phi$  are generally in agreement with the available experimental data in the studied collision centralities.

#### IV. THE ANISOTROPY FLOW OF SINGLE-CHARMED HADRONS

In this section, we study the  $v_2$  and  $v_3$  of single-charmed hadrons  $D^0$ ,  $D_s^+$ ,  $\Lambda_c^+$ ,  $\Xi_c^0$ ,  $\Omega_c^0$  at mid-rapidity in different centralities (0-10%, 10-30%, 30-50%) in Pb+Pb collisions at  $\sqrt{s_{NN}} = 2.76$  and 5.02 TeV.

##### A. THE ELLIPTIC FLOW OF SINGLE-CHARMED HADRONS

The  $v_2$  of single-charmed hadrons is also given by Eqs. (7) and (8). For the light-flavor quarks, the scaling coefficient  $a_4$  is approximated as 2 according to our previous analysis [42]. For charm quarks, although the exact value of  $a_4$  is not determined, the magnitude of the  $(a_4 - 2)v_{2,q}^2$  is estimated to be less than 0.4%. Therefore, we neglect the small contribution of quadratic terms of quark  $v_2$  and simplify the  $v_2$  of single-charmed hadrons as

$$v_{2,M_{c\bar{i}}}(p_T) \approx v_{2,q_c}(x_1 p_T) + v_{2,q_{\bar{i}}}(x_2 p_T), \quad (27)$$

$$v_{2,B_{c\ell\ell'}}(p_T) \approx v_{2,q_c}(x_1 p_T) + v_{2,q_{\ell}}(x_2 p_T) + v_{2,q_{\ell'}}(x_3 p_T). \quad (28)$$

We observe a simple sum rule for the  $v_2$  of charmed hadrons, which is convenient for experimental testing. Under the assumption of approximate isospin symmetry between up and down quarks (i.e.,  $v_{2,u} = v_{2,d}$ ), and strangeness neutrality (i.e.,  $v_{2,s} = v_{2,\bar{s}}$ ), the formulas for  $D^0$ ,  $D_s^+$ ,  $\Lambda_c^+$ ,  $\Xi_c^0$ , and  $\Omega_c^0$  can be further simplified using Eqs. (27) and

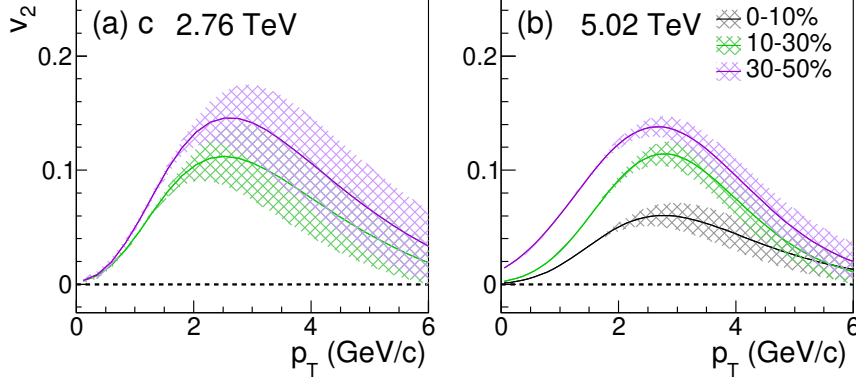


Figure 7.  $v_2$  of  $c$  quarks as a function of  $p_T$  in different centralities in Pb+Pb collisions at  $\sqrt{s_{NN}} = 2.76$  and 5.02 TeV.

(28) as follows

$$v_{2,D}(p_T) = v_{2,c} \left( \frac{r_{cu}}{1+r_{cu}} p_T \right) + v_{2,u} \left( \frac{1}{1+r_{cu}} p_T \right), \quad (29)$$

$$v_{2,D_s}(p_T) = v_{2,c} \left( \frac{r_{cs}}{1+r_{cs}} p_T \right) + v_{2,s} \left( \frac{1}{1+r_{cs}} p_T \right), \quad (30)$$

$$v_{2,\Lambda_c}(p_T) = v_{2,c} \left( \frac{r_{cu}}{2+r_{cu}} p_T \right) + 2v_{2,u} \left( \frac{1}{2+r_{cu}} p_T \right), \quad (31)$$

$$v_{2,\Xi_c}(p_T) = v_{2,c} \left( \frac{r_{cu}}{1+r_{su}+r_{cu}} p_T \right) + v_{2,u} \left( \frac{1}{1+r_{su}+r_{cu}} p_T \right) + v_{2,s} \left( \frac{r_{su}}{1+r_{su}+r_{cu}} p_T \right), \quad (32)$$

$$v_{2,\Omega_c}(p_T) = v_{2,c} \left( \frac{r_{cs}}{2+r_{cs}} p_T \right) + 2v_{2,s} \left( \frac{1}{2+r_{cs}} p_T \right). \quad (33)$$

Here, the relative momentum ratios are  $r_{cu} = m_c/m_u = 5$  and  $r_{cs} = m_c/m_s = 3$ . It can be seen that the  $v_2$  of charmed hadrons at  $p_T$  is the summation of the  $v_2$  of the charm quark whose  $p_T$  is close to that of the charmed hadron and the  $v_2$  of a light-flavor quark whose  $p_T$  is much smaller. This composition pattern is different from that of light-flavor hadrons where quarks have relatively close momentum.

Given the  $v_{2,u}$  and  $v_{2,s}$  obtained in the previous Sec. III A, the  $v_2$  of charm quarks can be extracted from the experimental data of  $D$  mesons,

$$v_{2,c}(p_T) = v_{2,D} \left( \frac{1+r_{cu}}{r_{cu}} p_T \right) - v_{2,u} \left( \frac{1}{r_{cu}} p_T \right). \quad (34)$$

For the charm quark, the parameterization form also adopts Eq. (18). In Fig. 7, we show the extracted  $v_{2,c}$  as a function of  $p_T$  in different centralities in Pb+Pb collisions at  $\sqrt{s_{NN}} = 2.76$  and 5.02 TeV. The shadow areas show the statistical uncertainties, which are passed from the statistical uncertainties of the experimental data for  $D^0$  [23, 26, 56]. It should be noted that this extraction method is only valid in the low and intermediate  $p_T$  region, where the combination mechanism dominates  $D$  meson production. In previous studies [16, 57–59], we found that the experimental data for  $p_T$  spectra of single-charmed hadrons in the  $p_T \lesssim 7.5$  GeV/c range from pp, p+Pb, and Pb+Pb collisions at LHC energies are well described by the EVC model. Therefore, the experimental data of  $v_2$  for  $D$  mesons with  $p_T \lesssim 7.5$  GeV/c can be used to extract the  $v_2$  of charm quarks with  $p_T \lesssim 6$  GeV/c within the EVC model. In the higher  $p_T$  region ( $p_T \gtrsim 7.5$  GeV/c), the fragmentation mechanism becomes significant [60, 61], and Eq. (34) is no longer applicable.

In Figs. 8–9, we present the results for the  $v_2$  of  $D^0$ ,  $D_s^+$ ,  $\Lambda_c^+$ ,  $\Xi_c^0$ , and  $\Omega_c^0$  at 0-10%, 10-30%, and 30-50% centralities in Pb+Pb collisions at  $\sqrt{s_{NN}} = 2.76$  and 5.02 TeV. The symbols are the experimental data [22–26] from the CMS and ALICE collaborations and lines are the calculated results. The results are in good agreement with the experimental data for  $D_s^+$  in Fig. 8(b). Predictions from QCM for other charmed baryons  $\Lambda_c^+$ ,  $\Xi_c^0$ ,  $\Omega_c^0$  are presented in Figs. 8(b)-(d) and 9(b)-(d), which can be tested in future experimental measurements.

Recently, ALICE collaboration report the preliminary data for  $v_2$  of single-charmed hadrons  $D^0$ ,  $D_s^+$ , and  $\Lambda_c^+$  in Pb+Pb collisions at  $\sqrt{s_{NN}} = 5.36$  TeV. Because of quite close collision energy, these data can be used as the first test of our prediction. In Fig. 10 we show these data in 30-50% centrality as well as  $v_2$  of  $D^0$  and  $D_s^+$  at  $\sqrt{s_{NN}} =$

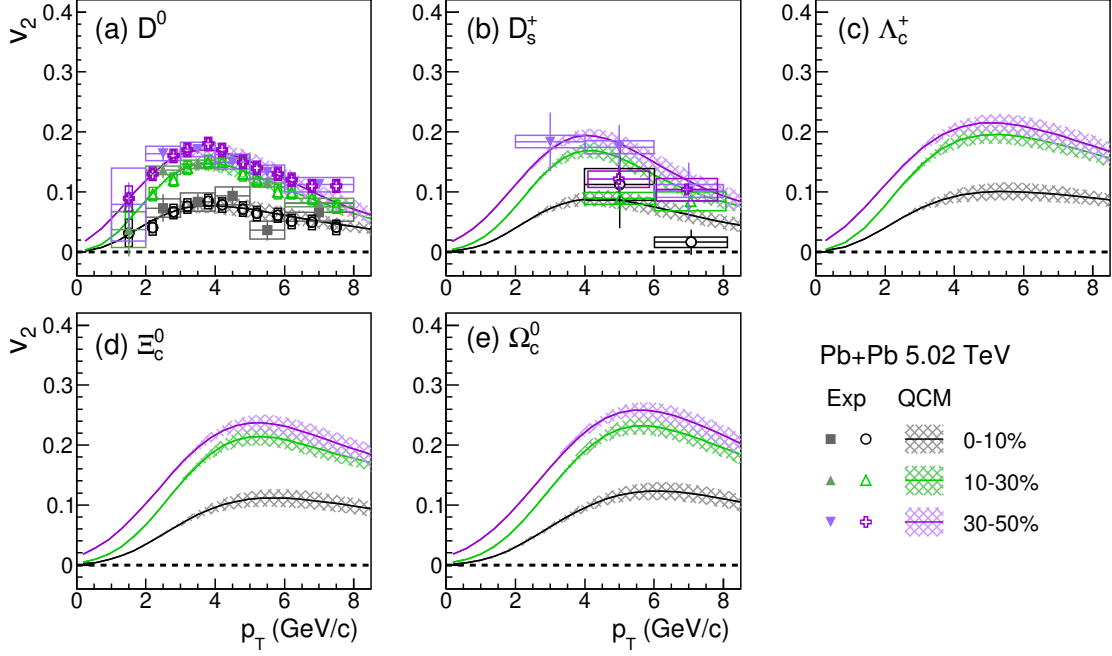


Figure 8. The  $v_2$  of (a)  $D^0$ , (b)  $D_s^+$ , (c)  $\Lambda_c^+$ , (d)  $\Xi_c^0$ , and (e)  $\Omega_c^0$  in different centralities in Pb+Pb collisions at  $\sqrt{s_{NN}} = 5.02$  TeV. Symbols are the experimental data [22–25] and lines are model results.

5.02 TeV. We see that  $v_2$  of  $D^0$  at the two collision energies are quite close with each other and  $v_2$  of  $D_s^+$  has a slight difference but the error bar at 5.02 TeV is large.

In order to clearly show the individual contributions of charm quarks and light-flavor quarks in the composition of  $v_2$  of charmed hadrons, we plot the contribution of charm quarks as the dot-dashed lines and that of light-flavor quarks as the dotted lines. The solid lines represent  $v_2$  of charmed hadrons in Fig. 10 (a)-(c). From Fig. 10 (a), we see that  $v_2$  of  $D^0$  in the range  $p_T \lesssim 2$  GeV/c is dominated by that of charm quarks and at large  $p_T$  the contribution of light-flavor quarks continuously strengthens and is even dominated at  $p_T \gtrsim 5$  GeV/c.  $v_2$  of  $D_s^+$  and  $\Lambda_c^+$  in Fig. 10 (b)-(c) also exhibit similar property. A difference between  $\Lambda_c^+$  and mesons  $D_s^+$  or  $D^0$  is that  $\Lambda_c^+$  contains double contribution from light-flavor quark  $v_2$ . Therefore, the  $v_2$  of  $\Lambda_c^+$  is larger than those of  $D_s^+$  or  $D^0$  at intermediate  $p_T$  but it does not follow the NCQ scaling exhibited in light-flavor hadrons because  $v_2$  of involved light-flavor quarks is quite different from  $v_2$  of charm quarks, see the crossing feature between the dotted line and dot-dashed line in Fig. 10 (a)-(c). Another related property for  $v_2$  of charmed meson and charmed baryon is that the peak position for  $v_2$  of  $\Lambda_c^+$  is at about 5 GeV/c while that of  $D^0$  is at about 3.5 GeV. This is because the double contribution from light-flavor quarks in  $\Lambda_c^+$  formation will push the peak position for  $v_2$  of  $\Lambda_c^+$  to larger  $p_T$  to a certain extent.

## B. THE TRIANGULAR FLOW OF SINGLE-CHARMED HADRONS

In this subsection, we study the  $v_3$  of single-charmed hadrons  $D^0$ ,  $D_s^+$ ,  $\Lambda_c^+$ ,  $\Xi_c^0$ , and  $\Omega_c^0$  in different centralities in Pb+Pb collisions at  $\sqrt{s_{NN}} = 5.02$  TeV, and make comparisons with the available experimental data [25, 56, 62].  $v_3$  of single-charmed hadrons in Eqs. (9) and (10) includes the small contribution from the quadratic terms of quark  $v_2$ . By NCQ scaling estimation for the second to fifth harmonic flows of light-flavor hadrons [10–14], the relating coefficient  $\frac{a_2}{a_3}$  is approximately 2.5 [46–49, 55]. Consequently, the magnitude of  $\left(\frac{a_2}{a_3} - 2\right)v_{2,q}^2$  is on the order of  $10^{-3}$ , and its influence is negligible in the formula. We therefore finally obtain

$$v_{3,M_{c\bar{c}}}(p_T) \approx v_{3,q_c}(x_1 p_T) + v_{3,q_l}(x_2 p_T), \quad (35)$$

$$v_{3,B_{c\ell\ell'}}(p_T) \approx v_{3,q_c}(x_1 p_T) + v_{3,q_l}(x_2 p_T) + v_{3,q_l'}(x_3 p_T), \quad (36)$$

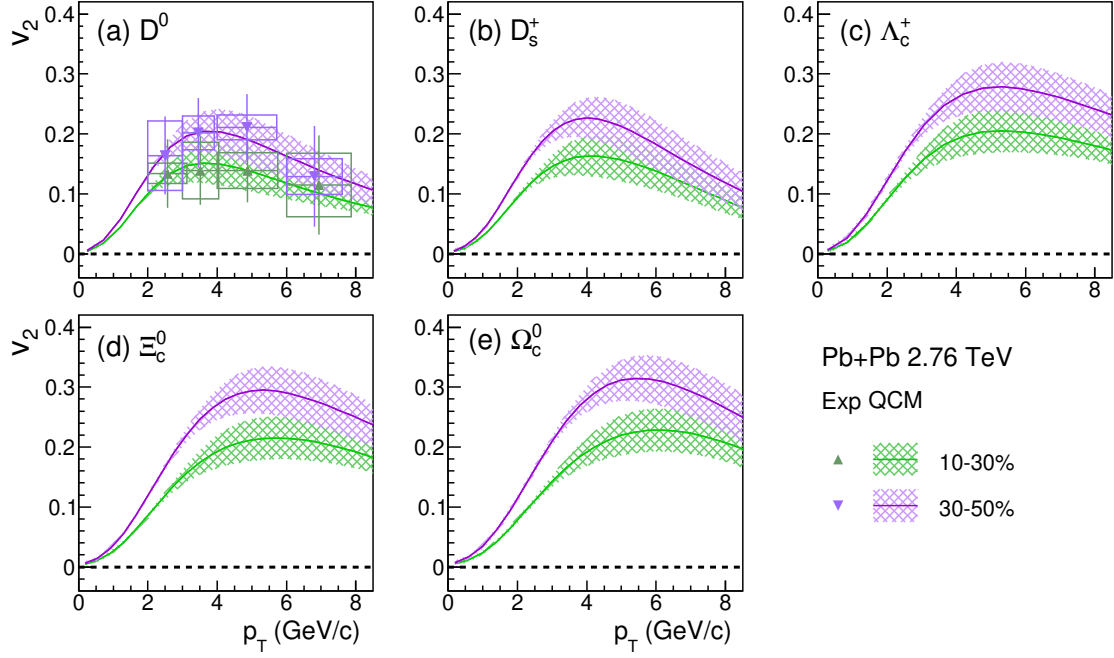


Figure 9. The  $v_2$  of (a)  $D^0$ , (b)  $D_s^+$ , (c)  $\Lambda_c^+$ , (d)  $\Xi_c^0$ , and (e)  $\Omega_c^0$  in different centralities in Pb+Pb collisions at  $\sqrt{s_{NN}} = 2.76$  TeV. Symbols are the experimental data [26] and lines are model results.

and obtain

$$v_{3,D}(p_T) = v_{3,c} \left( \frac{r_{cu}}{1+r_{cu}} p_T \right) + v_{3,u} \left( \frac{1}{1+r_{cu}} p_T \right), \quad (37)$$

$$v_{3,D_s}(p_T) = v_{3,c} \left( \frac{r_{cs}}{1+r_{cs}} p_T \right) + v_{3,s} \left( \frac{1}{1+r_{cs}} p_T \right), \quad (38)$$

$$v_{3,\Lambda_c}(p_T) = v_{3,c} \left( \frac{r_{cu}}{2+r_{cu}} p_T \right) + 2v_{3,u} \left( \frac{1}{2+r_{cu}} p_T \right), \quad (39)$$

$$v_{3,\Xi_c}(p_T) = v_{3,c} \left( \frac{r_{cu}}{1+r_{su}+r_{cu}} p_T \right) + v_{3,u} \left( \frac{1}{1+r_{su}+r_{cu}} p_T \right) + v_{3,s} \left( \frac{r_{su}}{1+r_{su}+r_{cu}} p_T \right), \quad (40)$$

$$v_{3,\Omega_c}(p_T) = v_{3,c} \left( \frac{r_{cs}}{2+r_{cs}} p_T \right) + 2v_{3,s} \left( \frac{1}{2+r_{cs}} p_T \right). \quad (41)$$

Here, we also adopt approximate isospin symmetry between up and down quarks, as well as strangeness neutrality between strange quarks and strange antiquarks at mid-rapidity in heavy-ion collisions at LHC energies.

We employ the procedure similar to that used in testing  $v_2$  of the single-charmed hadrons in the previous section to examine the  $v_3$  of the single-charmed hadrons. First, we again adopt Eq. (18) to parameterize the  $v_3$  of charm quarks. By fitting experimental data from  $D^0$  in Pb+Pb collisions at  $\sqrt{s_{NN}} = 5.02$  TeV, the values of the parameters  $v_{3,c}$  are extracted. Figure 11 shows the extracted  $v_{3,c}$  in the three centralities, where data from different centralities are scaled by different factors for clarity. Second, we use the resulting  $v_{3,c}$  and  $v_3$  of light-flavor quarks (i.e.,  $v_{3,u}, v_{3,s}$ ) obtained in Sec. III B to calculate the  $v_3$  of other single-charmed hadrons, such as  $D_s^+$ ,  $\Lambda_c^+$ ,  $\Xi_c^0$ , and  $\Omega_c^0$  by Eqs. (38)-(41), and compare them with experimental data.

Fig. 12 shows the results of the  $v_3$  of  $D^0$ ,  $D_s^+$ ,  $\Lambda_c^+$ ,  $\Xi_c^0$ , and  $\Omega_c^0$  in Pb+Pb collisions at  $\sqrt{s_{NN}} = 5.02$  TeV in the 0-10%, 10-30%, and 30-50% centralities. Comparing Eqs. (37)-(41) for  $v_3$  and Eqs. (29)-(33) for  $v_2$  of charmed hadrons, we see that the composition pattern of charm quarks and light-flavor quarks are very similar in  $v_2$  and  $v_3$  of charmed hadrons. Therefore, like those shown in Fig. 10 for hadronic  $v_2$ ,  $v_3$  of charmed hadrons in the range  $p_T \lesssim 4$  GeV/c is dominated by  $v_3$  of charm quarks and in the intermediate  $p_T$  region ( $4 \lesssim p_T \lesssim 7.5$  GeV/c), the contribution from light-flavor quarks gradually increases. Taking results in 30-50% centrality as an example, we see that the peak position for  $v_3$  of  $D^0$ ,  $D_s^+$  is located at about 4.0 GeV/c while that of baryons  $\Lambda_c^+$ ,  $\Xi_c^0$ , and  $\Omega_c^0$  is located at about 5.5 GeV/c. The maximum  $v_3$  value of  $\Lambda_c^+$  at peak position is higher than that of  $D^0$  about 0.07 because of an extra contribution of light-flavor quark  $v_3$ . The maximum  $v_3$  of strange charmed hadrons  $D_s^+$ ,  $\Xi_c^0$ , and  $\Omega_c^0$  are higher than

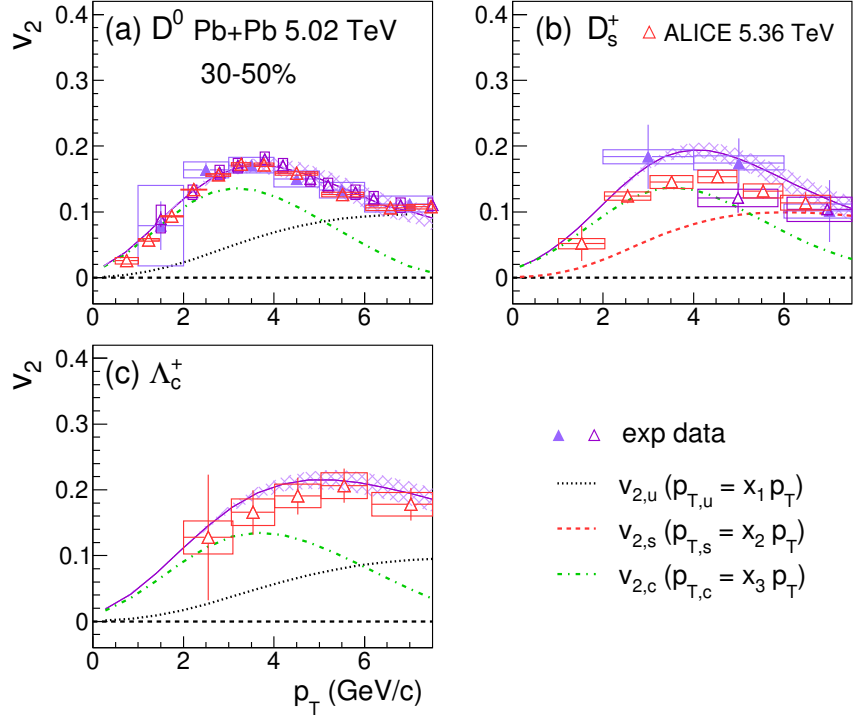


Figure 10. The  $v_2$  of (a)  $D^0$ , (b)  $D_s^+$ , and (c)  $\Lambda_c^+$  in 30-50% centrality in Pb+Pb collisions at  $\sqrt{s_{NN}} = 5.02$  and 5.36 TeV. Symbols are the experimental data [22–25] and lines are model results.

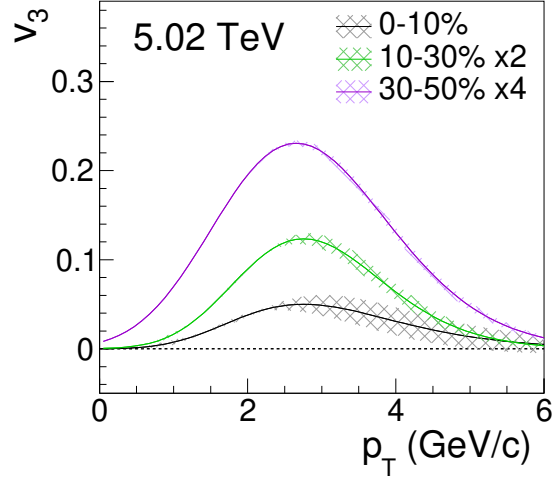


Figure 11.  $v_3$  of  $c$  quarks as a function of  $p_T$  in different centralities in Pb+Pb collisions at  $\sqrt{s_{NN}} = 5.02$  TeV.

those of  $D^0$  and  $\Lambda_c^+$  because of the involved strange quarks have larger transverse momentum and thus larger  $v_3$  at charm quark hadronization. These properties of  $v_3$  of charmed hadrons are left for future test.

### C. THE PROPERTIES OF $v_2$ AND $v_3$ OF QUARKS

In this subsection, we utilize the previously obtained  $v_2$  and  $v_3$  of up/down quarks, strange quarks and charm quarks just before hadronization to further investigate their properties, with a particular focus on the scaling behavior of anisotropic flow at different orders.

In Section II, we assumed a scaling relation  $v_{n,q} = a_n v_{2,q}^{n/2}$  at quark level to estimate the contribution of higher-order quark flows to the lower-order anisotropic flow of single-charmed hadrons. Here, we test this relation using the

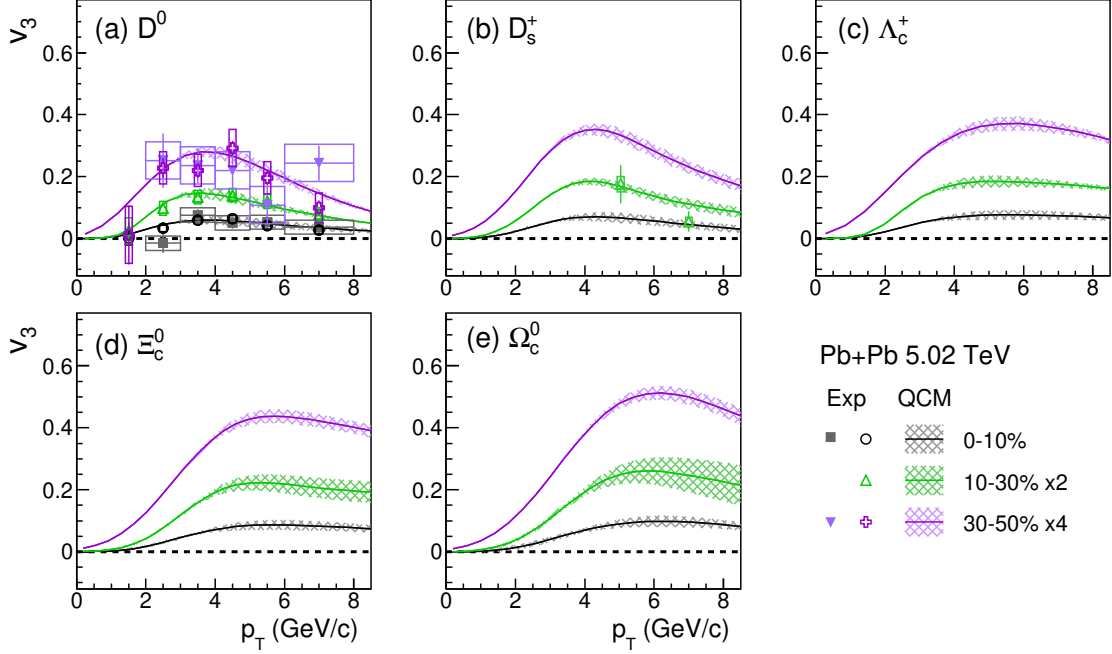


Figure 12. The  $v_3$  of (a)  $D^0$ , (b)  $D_s^+$ , (c)  $\Lambda_c^+$ , (d)  $\Xi_c^0$ , and (e)  $\Omega_c^0$  in different centralities in Pb+Pb collisions at  $\sqrt{s_{NN}} = 5.02$  TeV. Symbols are the experimental data [25, 56, 62] and lines are model results.

obtained  $v_2$  and  $v_3$  of up/down, strange, and charm quarks. The results of  $a_3 = v_3/v_2^{3/2}$  as a function of  $p_T$  are shown in Fig. 13. We observe that the values of  $a_3$  for up, strange, and charm quarks all exhibit a weak dependence on  $p_T$ , clustering around a value of approximately 2~4. The same behavior is also seen at RHIC. Moreover, the value of  $a_3$  for charm quarks is observed to be significantly smaller than those for light-flavor quarks in the three centralities. This may be explained by the observation that heavier quarks exhibit a more pronounced centrality dependence in their elliptic flow, whereas triangular flow shows relatively little sensitivity to centrality variations. These results validate the consistency of the scaling relation  $v_{n,q} = a_n v_{2,q}^{n/2}$  as used in the current model for analyzing the anisotropic flow  $v_n$  of single-charmed hadrons. The observed scaling behavior of quark flows can be qualitatively understood within the framework of hydrodynamic evolution of hot quark matter [51, 63].

## V. SUMMARY

In this paper, we have applied the constituent quark equal-velocity combination model to study  $v_2$  and  $v_3$  of light-flavor hadrons and single-charmed hadrons in different centralities (0-10%, 10-30%, and 30-50%) in Pb+Pb collisions at  $\sqrt{s_{NN}} = 2.76$  and 5.02 TeV. In equal velocity combination mechanism, the  $v_{2,3}$  of hadrons can be finally expressed as the linear superposition of  $v_{2,3}$  of constituent quarks and antiquarks after neglecting the higher order flows of quarks. These simplified analytical expressions for hadronic flows are conveniently tested by experimental data.

Using these analytical expressions for hadronic flows, we firstly systematically study the  $v_2$  and  $v_3$  of  $p$ ,  $\Lambda$ ,  $\Xi$ ,  $\Omega$ , and  $\phi$  in different centralities in Pb+Pb collisions at  $\sqrt{s_{NN}} = 2.76$  and 5.02 TeV.  $v_2$  and  $v_3$  of quarks are obtained by combination fitting to experimental data of  $\Lambda$  and  $\Xi$ , and we used them to calculate flows of other hadrons and compare them with the available experimental data. We found good agreement with data at  $\sqrt{s_{NN}} = 2.76$ . In Pb+Pb collisions at  $\sqrt{s_{NN}} = 5.02$  TeV, we found that  $v_2$  data of  $\phi$  are higher than our predictions by  $s\bar{s}$  quark combination. We therefore considered the possible contribution of final-state hadronic rescattering by including the production of  $\phi$  via two-kaon coalescence. We found that two-kaon coalescence channel contributes about 20% of  $\phi$  production at  $\sqrt{s_{NN}} = 5.02$  TeV. With this contribution estimation, we further predict  $v_3$  of  $\phi$  as the function of  $p_T$  for future test.

Using the obtained  $v_2$  and  $v_3$  of light-flavor quarks in studying light-flavor hadrons, we further studied the  $v_2$  and  $v_3$  of single-charmed hadrons in Pb+Pb collisions at  $\sqrt{s_{NN}} = 2.76$  and 5.02 TeV. We used the experimental data of  $D^0$  to fix the  $v_2$  and  $v_3$  of charm quarks and then applied EVC model to predicted flows of  $D_s^+$ ,  $\Lambda_c^+$ ,  $\Xi_c^0$ , and  $\Omega_c^0$  at two collision energies. We also took the preliminary data of  $D^0$ ,  $D_s^+$ , and  $\Lambda_c^+$  in 30-50% centrality in Pb+Pb collisions

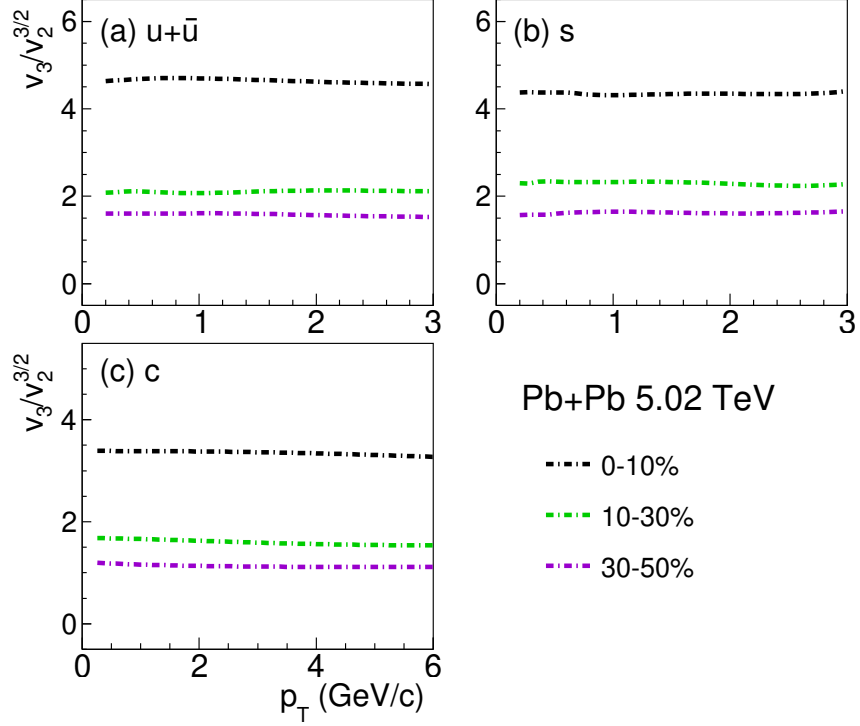


Figure 13. The ratio  $v_3/v_2^{3/2}$  of quarks as a function of  $p_T$  in different centralities in Pb+Pb collisions at  $\sqrt{s_{NN}} = 5.02$  TeV.

at  $\sqrt{s_{NN}} = 5.36$  TeV to compare with our predictions to show some features of  $v_2$  of charmed hadron, see Fig. 10. An interesting feature is that  $v_2$  of  $\Lambda_c^+$  is only slightly higher than those of  $D^0$  and  $D_s^+$  in small and intermediate  $p_T$  ranges, which is different from the NCQ scaling property for light-flavor hadrons. This is because in EVC model charm quark hadronizes by capturing a light-flavor antiquark or two light-flavor quarks with much smaller momentum  $p_{T,q} = m_q/m_c p_{T,c} \approx 0.2 - 0.3 p_{T,c}$ .  $v_2$  of charmed hadrons at  $p_T$  is therefore the summation of  $v_2$  of charm quark at a slightly smaller  $p_T$  and that of light-flavor quarks at a much smaller  $p_T$  which has quite small value at low  $p_T$ . Another property is that the  $p_T$  position for the maximum  $v_2$  of  $\Lambda_c^+$  is larger than that of D mesons about 1 GeV/c. This is because in  $\Lambda_c^+$  formation a charm quark will capture two light-flavor quarks and  $v_2$  of light-flavor quarks involving  $\Lambda_c^+$  formation is ascending function with  $p_T$ .

In deriving  $v_2$  and  $v_3$  of hadrons, we assumed a scaling relation  $v_{n,q} = a_n (v_{2,q})^{n/2}$  for quark flows. Using the obtained  $v_2$  and  $v_3$  of light-flavor quarks and charm quarks, we found that this relation holds well for  $v_3$  of light-flavor quarks and charm quarks at the two LHC energies. This was consistent with our previous results at RHIC energies [42]. The origin of this scaling relation for quark flows is related to hydrodynamic expansion evolution of QGP created in relativistic heavy-ion collisions.

## VI. ACKNOWLEDGMENTS

This work was supported in part by Shandong Provincial Natural Science Foundation (Grant Nos. ZR2025QC38 and ZR2025MS01), and the National Natural Science Foundation of China under Grants No. 12375074 and 12175115.

- 
- [1] E. V. Shuryak, *Phys. Lett. B* **78**, 150 (1978).  
[2] E. V. Shuryak, *Phys. Rept.* **61**, 71 (1980).  
[3] J.-Y. Ollitrault, *Phys. Rev. D* **46**, 229 (1992).  
[4] S. Voloshin and Y. Zhang, *Z. Phys. C* **70**, 665 (1996), arXiv:hep-ph/9407282.  
[5] A. M. Poskanzer and S. A. Voloshin, *Phys. Rev. C* **58**, 1671 (1998), arXiv:nucl-ex/9805001.  
[6] P. F. Kolb, *Phys. Rev. C* **68**, 031902 (2003), arXiv:nucl-th/0306081.

- [7] P. F. Kolb, J. Sollfrank, and U. W. Heinz, *Phys. Rev. C* **62**, 054909 (2000), arXiv:hep-ph/0006129.
- [8] P. Huovinen, P. F. Kolb, U. W. Heinz, P. V. Ruuskanen, and S. A. Voloshin, *Phys. Lett. B* **503**, 58 (2001), arXiv:hep-ph/0101136.
- [9] D. Teaney, J. Lauret, and E. V. Shuryak, *Phys. Rev. Lett.* **86**, 4783 (2001), arXiv:nucl-th/0011058.
- [10] L. Adamczyk *et al.* (STAR), *Phys. Rev. C* **88**, 014902 (2013), arXiv:1301.2348 [nucl-ex].
- [11] A. Adare *et al.* (PHENIX), *Phys. Rev. Lett.* **98**, 162301 (2007), arXiv:nucl-ex/0608033.
- [12] L. Adamczyk *et al.* (STAR), *Phys. Rev. Lett.* **116**, 062301 (2016), arXiv:1507.05247 [nucl-ex].
- [13] B. B. Abelev *et al.* (ALICE), *JHEP* **06**, 190, arXiv:1405.4632 [nucl-ex].
- [14] S. Acharya *et al.* (ALICE), *JHEP* **09**, 006, arXiv:1805.04390 [nucl-ex].
- [15] V. Greco, C. M. Ko, and P. Levai, *Phys. Rev. Lett.* **90**, 202302 (2003), arXiv:nucl-th/0301093.
- [16] W.-b. Chang, R.-q. Wang, J. Song, F.-l. Shao, Q. Wang, and Z.-t. Liang, *Symmetry* **15**, 400 (2023), arXiv:2302.07546 [nucl-th].
- [17] R. J. Fries, B. Muller, C. Nonaka, and S. A. Bass, *Phys. Rev. Lett.* **90**, 202303 (2003), arXiv:nucl-th/0301087.
- [18] V. Greco, C. M. Ko, and P. Levai, *Phys. Rev. C* **68**, 034904 (2003), arXiv:nucl-th/0305024.
- [19] R. J. Fries, B. Muller, C. Nonaka, and S. A. Bass, *Phys. Rev. C* **68**, 044902 (2003), arXiv:nucl-th/0306027.
- [20] D. Molnar and S. A. Voloshin, *Phys. Rev. Lett.* **91**, 092301 (2003), arXiv:nucl-th/0302014.
- [21] V. Minissale, F. Scardina, and V. Greco, *Phys. Rev. C* **92**, 054904 (2015), arXiv:1502.06213 [nucl-th].
- [22] A. M. Sirunyan *et al.* (CMS), *Phys. Lett. B* **816**, 136253 (2021), arXiv:2009.12628 [hep-ex].
- [23] S. Acharya *et al.* (ALICE), *JHEP* **10**, 141, arXiv:2005.14518 [nucl-ex].
- [24] S. Acharya *et al.* (ALICE), *Phys. Lett. B* **827**, 136986 (2022), arXiv:2110.10006 [nucl-ex].
- [25] Azimuthal anisotropy of prompt  $D_s$  mesons at  $\sqrt{s_{NN}} = 5.02$  TeV with CMS experiment (2025).
- [26] R. Bailhache (ALICE), *Nucl. Phys. A* **931**, 530 (2014).
- [27] N. R. Saha (CMS), *Nuovo Cim. C* **48**, 20 (2024).
- [28] N. R. Saha (CMS), *J. Subatomic Part. Cosmol.* **4**, 100095 (2025).
- [29] S. Acharya *et al.* (ALICE), *JHEP* **05**, 243, arXiv:2206.04587 [nucl-ex].
- [30] Y. Zhu (ALICE), *PoS ICHEP2018*, 441 (2019).
- [31] N. Mallick, S. Prasad, A. N. Mishra, R. Sahoo, and G. G. Barnaföldi, *Phys. Rev. D* **107**, 094001 (2023), arXiv:2301.10426 [hep-ph].
- [32] S. Tang, Z. Zhang, C. Zhang, L. Zheng, and R. Wan, *Chin. Phys.* **49**, 124104 (2025), arXiv:2507.05596 [hep-ph].
- [33] M. Alqahtani, M. Nopoush, R. Ryblewski, and M. Strickland, *Phys. Rev. C* **96**, 044910 (2017), arXiv:1705.10191 [nucl-th].
- [34] H. Alalawi, M. Alqahtani, and M. Strickland, *Symmetry* **14**, 329 (2022), arXiv:2112.14597 [nucl-th].
- [35] X. Zhu, *Adv. High Energy Phys.* **2016**, 4236492 (2016), arXiv:1607.04003 [nucl-th].
- [36] A. Akhil and S. K. Tiwari, *J. Phys. G* **51**, 035002 (2024), arXiv:2309.06128 [hep-ph].
- [37] S. Grigoryan, *Phys. Rev. C* **113**, 014903 (2026), arXiv:2509.01807 [hep-ph].
- [38] G. Devi, A. Singh, S. Pandey, and B. K. Singh, *Eur. Phys. J. Plus* **138**, 921 (2023), arXiv:2306.02276 [hep-ph].
- [39] G. Devi and B. K. Singh, *Phys. Rev. C* **112**, 034907 (2025), arXiv:2409.10435 [hep-ph].
- [40] J. Song, H.-h. Li, and F.-l. Shao, *Eur. Phys. J. C* **81**, 5 (2021), arXiv:2008.03017 [nucl-th].
- [41] J. Song, X.-r. Gou, F.-l. Shao, and Z.-T. Liang, *Phys. Lett. B* **774**, 516 (2017), arXiv:1707.03949 [hep-ph].
- [42] Y.-t. Feng, R.-q. Wang, F.-l. Shao, and J. Song, *Phys. Rev. C* **111**, 064902 (2025), arXiv:2503.16804 [hep-ph].
- [43] R.-Q. Wang, X.-L. Hou, Y.-H. Li, J. Song, and F.-L. Shao, *Nucl. Sci. Tech.* **36**, 185 (2025), arXiv:2408.06384 [hep-ph].
- [44] B. I. Abelev *et al.* (STAR), *Phys. Rev. Lett.* **101**, 252301 (2008), arXiv:0807.1518 [nucl-ex].
- [45] B. Abelev *et al.* (ALICE), *Phys. Rev. Lett.* **111**, 232302 (2013), arXiv:1306.4145 [nucl-ex].
- [46] J. Adams *et al.* (STAR), *Phys. Rev. C* **72**, 014904 (2005), arXiv:nucl-ex/0409033.
- [47] B. I. Abelev *et al.* (STAR), *Phys. Rev. C* **75**, 054906 (2007), arXiv:nucl-ex/0701010.
- [48] P. F. Kolb, L.-W. Chen, V. Greco, and C. M. Ko, *Phys. Rev. C* **69**, 051901 (2004), arXiv:nucl-th/0402049.
- [49] L.-W. Chen, C. M. Ko, and Z.-W. Lin, *Phys. Rev. C* **69**, 031901 (2004), arXiv:nucl-th/0312124.
- [50] F. G. Gardim, F. Grassi, M. Luzum, and J.-Y. Ollitrault, *Phys. Rev. Lett.* **109**, 202302 (2012), arXiv:1203.2882 [nucl-th].
- [51] N. Borghini and J.-Y. Ollitrault, *Phys. Lett. B* **642**, 227 (2006), arXiv:nucl-th/0506045.
- [52] C. Gombeaud and J.-Y. Ollitrault, *Phys. Rev. C* **81**, 014901 (2010), arXiv:0907.4664 [nucl-th].
- [53] C. Alt *et al.* (NA49), *Phys. Rev. C* **78**, 044907 (2008), arXiv:0806.1937 [nucl-ex].
- [54] L.-X. Sun, R.-Q. Wang, J. Song, and F.-L. Shao, *Chin. Phys. C* **36**, 55 (2012), arXiv:1105.0577 [hep-ph].
- [55] V. Bairathi (STAR), *J. Phys. Conf. Ser.* **668**, 012039 (2016).
- [56] A. M. Sirunyan *et al.* (CMS), *Phys. Rev. Lett.* **120**, 202301 (2018), arXiv:1708.03497 [nucl-ex].
- [57] J. Song, H.-h. Li, and F.-l. Shao, *Eur. Phys. J. C* **83**, 852 (2023), arXiv:2304.00434 [hep-ph].
- [58] H.-H. Li, F.-L. Shao, J. Song, and R.-Q. Wang, *Phys. Rev. C* **97**, 064915 (2018), arXiv:1712.08921 [hep-ph].
- [59] J. Song, H.-h. Li, and F.-l. Shao, *Eur. Phys. J. C* **78**, 344 (2018), arXiv:1801.09402 [hep-ph].
- [60] Y. Oh, C. M. Ko, S. H. Lee, and S. Yasui, *Phys. Rev. C* **79**, 044905 (2009), arXiv:0901.1382 [nucl-th].
- [61] S. Cao, G.-Y. Qin, and S. A. Bass, *Phys. Rev. C* **92**, 024907 (2015), arXiv:1505.01413 [nucl-th].
- [62] S. Acharya *et al.* (ALICE), *Phys. Lett. B* **813**, 136054 (2021), arXiv:2005.11131 [nucl-ex].
- [63] E. Retinskaya, M. Luzum, and J.-Y. Ollitrault, *Phys. Rev. C* **89**, 014902 (2014), arXiv:1311.5339 [nucl-th].